16th World Congress in Computational Mechanics (WCCM)
21-26 July 2024, Vancouver, Canada
A. Korobenko, M. Laforest, S. Prudhomme, R. Vaziri (Eds)

AN IMPROVED FLUX VECTOR SPLITTING METHOD FOR CHARACTERISTIC-WISE WENO SCHEMES OF THE EULER EQUATIONS

Jianyu Qin[1,2], **Yiqing Shen**[1,2]

[1] State Key Laboratory of High Temperature Gas Dynamics, Institute of Mechanics, Chinese Academy of Sciences, Beijing 100049, China

[2] School of Engineering Science, University of Chinese Academy of Sciences, Beijing 100049, China

Key words: Flux vector splitting (FVS), WENO, Characteristic-wise reconstruction, Contact discontinuity.

Abstract. Steger-Warming (SW) [1] and Lax-Friedrich-type (LF) [2] flux vector splitting methods are used extensively by shock capturing WENO schemes in varieties of compressible flow simulations. Due to the less dissipation, the SW method is preferred in flow calculations that require fine scale structures such as direct numerical simulation of turbulence. However, this paper shows that, even if the characteristic-wise WENO scheme is used, the SW method may still exhibit some oscillations near contact discontinuities, while the LF method does not. Analysis similar to the reference [3] shows that, using the SW method may make the characteristic-wise WENO scheme become close the component-wise WENO scheme near subsonic contact discontinuities. Based on that, an improved flux vector splitting method, which adjusts the eigenvalues of the flux vector splitting in the characteristic-wise WENO procedure, is proposed to obtain the low-dissipation property and prevent contact discontinuity oscillations at the same time. Numerical experiments are performed to validate and evaluate the new method. Numerical results show that the proposed method keeps the non-oscillatory flow field near discontinuities as LF method and also avoids smearing out other flow regions, similar to the SW method.

1 INTRODUCTION

For the Euler systems of the gas dynamics, Jiang and Shu [4] proposed the characteristic-wise WENO scheme. The flux is first split into positive and negative parts, and then the local characteristic fields (is defined as the production of the left-eigenvectors matrix of the Jacobian matrix and the split flux) at each interface (for example, at the interface $j+1/2$, the local characteristic fields for a 5th-order WENO scheme are needed on the stencil $S=(j-2,j-1,...,j+3)$) are calculated. The characteristic-wise WENO reconstructions at the interface $j+1/2$ are obtained by using the scalar WENO scheme for each component of the characteristic

fields. Finally, by multiplying with the right-eigenvectors matrix, we get the numerical fluxes for the Euler systems.

There are many methods were proposed for spitting the flux vector. The Steger-Warming flux vector splitting (SW-FVS) method [1] is one of the popular methods and has been extensively applied in computational fluid dynamics. However, for some extreme cases, the high order SW-FVS method may generate some issues, such as numerical oscillations and unstability. While, the Lax-Friedrich flux vector splitting (LF-FVS) method [2] utilized the maximum eigenvalue of the Jacobian matrix has simple form and strong robustness and hence has also been used in many studies. Compared with the SW-FVS method, the LF-FVS method has been demonstrated to be more dissipative.

For resolving the contact discontinuities, Johnsen [5] analyzed the reason of the velocity and pressure oscillations caused by the LF solver with component-wise WENO reconstruction, and proposed to use the reconstruction of the primitive variables or the reconstruction of the characteristic variables to suppress this kind of oscillations. He et al.[5] analyzed the component-wise WENO-FVS method, and proposed to combine the global LF-FVS (GLF-FVS) method with a consistent discretization between different equations to reduce the velocity and pressure oscillations. Although the characteristic-wise WENO reconstruction based the FVS methods were developed earlier, there is seldom analysis about resolving the contact discontinuity problem.

In this paper, we analyze the characteristic-wise WENO scheme of the FVS (SW and GLF) methods. It shows that, for the case of subsonic contact discontinuity, the characteristic-wise WENO scheme based on the SW-FVS method becomes close to the component-wise WENO scheme and produces oscillatory distribution of density. Then, we propose a characteristic-wise WENO reconstruction based on the hybrid FVS method of SW-FVS and GLF-FVS. That is, in the first step of the characteristic-wise reconstruction, we identify if the global stencil (for example, the global stencil $S = (j-2, j-1, ..., j+3)$ is used for the 5th-order WENO scheme) includes the density discontinuity in the subsonic region, then the GLF-FVS method is used to get the split flux vector just for calculating the local characteristic fields on this stencil. And SW-FVS method is used for other stencils. The hybrid method for the characteristic-wise reconstruction can keep the ENO property as that of GLF-FVS method and has low-dissipation in smooth regions as that of SW-FVS method.

2 NUMERICAL ALGORITHM

The one-dimensional Euler equations are taken as an example to describe the WENO schemes for the governing equations of gas dynamics,

$$\frac{\partial \mathbf{U}}{\partial t} + \frac{\partial \mathbf{F}}{\partial x} = 0, \tag{1}$$

$$\mathbf{U} = \begin{bmatrix} \rho \\ \rho u \\ E \end{bmatrix}, \mathbf{F} = \begin{bmatrix} \rho u \\ \rho u^2 + p \\ (E+p)u \end{bmatrix}, \tag{2}$$

and the equation of state is

$$p = (\gamma - 1)\left(E - \frac{1}{2}\rho u^2\right), \tag{3}$$

where ρ, u, E and p are the density, velocity, total energy and pressure, respectively, γ is the ratio of specific heat.

According to the hyperbolic character of the Euler system, there are

$$\mathbf{F} = \mathbf{A}\mathbf{U}, \mathbf{A} = \frac{\partial \mathbf{F}}{\partial \mathbf{U}}, \mathbf{A} = \mathbf{R}\Lambda\mathbf{L}, \tag{4}$$

where, $\mathbf{\Lambda}$ is the diagonal matrix of the eigenvalues of the Jacobian matrix $\mathbf{A}$, $\mathbf{\Lambda} = \mathrm{diag}\,(\lambda_1, \lambda_2, \lambda_3) = \mathrm{diag}(u - c, u, u + c)$, $c = \sqrt{\gamma p/\rho}$ is the speed of sound, and $\mathbf{R}$ and $\mathbf{L}$ are the matrices of the right and left eigenvectors, respectively. For convenience, here we give the formulations of the matrices $\mathbf{A}, \mathbf{R}$ and $\mathbf{L}$,

$$\begin{aligned}
\mathbf{A} &= \begin{bmatrix} 0 & 1 & 0 \\ \frac{\gamma-3}{2}u^2 & (3-\gamma)u & \gamma - 1 \\ \frac{\gamma-1}{2}u^3 - uH & H - (\gamma-1)u^2 & \gamma u \end{bmatrix}, \mathbf{R} = \begin{bmatrix} 1 & 1 & 1 \\ u - c & u & u + c \\ H - uc & \frac{1}{2}u^2 & H + uc \end{bmatrix}, \\
\mathbf{L} = \mathbf{R}^{-1} &= \begin{bmatrix} \frac{1}{2}\left(\frac{\gamma-1}{2c^2}u^2 + \frac{u}{c}\right) & -\frac{1}{2}\left(\frac{\gamma-1}{c^2}u + \frac{1}{c}\right) & \frac{\gamma-1}{2c^2} \\ 1 - \frac{\gamma-1}{2c^2}u^2 & \frac{\gamma-1}{c^2}u & -\frac{\gamma-1}{c^2} \\ \frac{1}{2}\left(\frac{\gamma-1}{2c^2}u^2 - \frac{u}{c}\right) & -\frac{1}{2}\left(\frac{\gamma-1}{c^2}u - \frac{1}{c}\right) & \frac{\gamma-1}{2c^2} \end{bmatrix},
\end{aligned} \tag{5}$$

with the enthalpy $H = (E + p)/\rho$.

2.1 The flux vector splitting methods for Euler equations

The flux $\mathbf{F}$ can be split into positive and negative parts as $\mathbf{F} = \mathbf{F}^+ + \mathbf{F}^-$,

$$\mathbf{F}^{\pm} = \mathbf{A}^{\pm}\mathbf{U}, \quad \mathbf{A}^{\pm} = \mathbf{R}\mathbf{\Lambda}^{\pm}\mathbf{L}, \tag{6}$$

where the eigenvalues matrices $\mathbf{\Lambda}^+ = \mathrm{diag}\left(\lambda_1^+, \lambda_2^+, \lambda_3^+\right)$ and $\mathbf{\Lambda}^- = \mathrm{diag}\left(\lambda_1^-, \lambda_2^-, \lambda_3^-\right)$ with $\lambda_k^+ \geq 0, \lambda_k^- \leq 0 (k = 1, 2, 3)$, and $\mathbf{\Lambda} = \mathbf{\Lambda}^+ + \mathbf{\Lambda}^-$. The generalized formulations of the split fluxes can be written as

$$\mathbf{F}^{\pm} = \begin{bmatrix} f_1^{\pm} \\ f_2^{\pm} \\ f_3^{\pm} \end{bmatrix} = \frac{\rho}{2\gamma} \begin{bmatrix} \lambda_1^{\pm} + 2(\gamma-1)\lambda_2^{\pm} + \lambda_3^{\pm} \\ (u-c)\lambda_1^{\pm} + 2u(\gamma-1)\lambda_2^{\pm} + (u+c)\lambda_3^{\pm} \\ (H-uc)\lambda_1^{\pm} + u^2(\gamma-1)\lambda_2^{\pm} + (H+uc)\lambda_3^{\pm} \end{bmatrix}. \tag{7}$$

There are many methods to carry out Eq. (7). For example, in the Steger-Warming (SW) flux vector splitting method [1], the eigenvalues are calculated as

$$\lambda_k^{\pm} = \frac{1}{2}\left(\lambda_k \pm |\lambda_k|\right), \tag{8}$$

the global Lax-Friedrichs (GLF) splitting method [2] takes

$$\lambda_k^{\pm} = \frac{1}{2}\left(\lambda_k \pm \alpha\right), \tag{9}$$

where α is the maximal eigenvalue over the whole computational domain. Clearly, the global Lax-Friedrichs splitting method has a simple form as

$$\mathbf{F}^{\pm} = \begin{bmatrix} f_1^{\pm} \\ f_2^{\pm} \\ f_3^{\pm} \end{bmatrix} = \frac{1}{2}\begin{bmatrix} \rho u \pm \alpha\rho \\ \rho u^2 + p \pm \alpha\rho u \\ (E+p)u \pm \alpha E \end{bmatrix}. \tag{10}$$

2.2 The WENO schemes

The semi-discrete form of Eq. (1) on the equally spaced grid (with $\Delta x = x_{j+1} - x_j$) can be written as

$$\frac{\partial \mathbf{U}}{\partial t} = -\frac{\mathbf{F}_{j+1/2} - \mathbf{F}_{j-1/2}}{\Delta x}, \tag{11}$$

where $\mathbf{F}_{j+1/2} = \mathbf{F}^+_{j+1/2} + \mathbf{F}^-_{j+1/2}$ is the numerical flux at cell interface $j + 1/2$.

For simplicity, the superscript $\pm$ is dropped. A scalar flux f is used to briefly introduce the WENO schemes. The general numerical flux of a fifth-order WENO [4] scheme can be written as

$$f_{j+1/2} = \sum_{k=0}^{2} \omega_k q_k, \tag{12}$$

where q_k is the third-order flux on the sub-stencil $S_k = (x_{i+k-2}, x_{i+k-1}, \ldots, x_{i+k})$ and given by

$$\begin{cases} q_0 = \frac{1}{3}f_{j-2} - \frac{7}{6}f_{j-1} + \frac{11}{6}f_j, \\ q_1 = -\frac{1}{6}f_{j-1} + \frac{5}{6}f_j + \frac{1}{3}f_{j+1}, \\ q_2 = \frac{1}{3}f_j + \frac{5}{6}f_{j+1} - \frac{1}{6}f_{j+2}. \end{cases} \tag{13}$$

The weight ω_k of WENO-JS scheme [4] is calculated as

$$\omega_k = \frac{\alpha_k}{\alpha_0 + \alpha_1 + \alpha_2}, \quad \alpha_k = \frac{c_k}{\left(\beta_k + \varepsilon\right)^2}, \quad k = 0, 1, 2, \tag{14}$$

where β_k is the local smoothness indicator (LSI) used to measure the relative smoothness of a solution on the substencil S_k. Constants $c_0 = 0.1, c_1 = 0.6$ and $c_2 = 0.3$ are the optimal weights, which generate the fifth-order upstream scheme. The parameter ε is a positive real number introduced to avoid the denominator becoming zero and $\varepsilon = 10^{-6}$ is suggested by Jiang and Shu [4]. The classical local smoothness indicator (LSI) proposed by Jiang and Shu is given by

$$\beta_k = \sum_{l=1}^{r-1} \int_{x_{i-1/2}}^{x_{i+1/2}} (\Delta x)^{2l-1} \left(q_k^{(n)}\right)^2 dx, \tag{15}$$

where $q_k^{(n)}$ is the n th order derivative of $q_k(x)$, and $q_k(x)$ is the interpolation polynomial on sub-stencil S_k. For the fifth-order WENO scheme $(r = 3)$, Eq. (15) gives

$$\begin{cases} \beta_0 = \frac{13}{12}\left(f_{j-2} - 2f_{j-1} + f_j\right)^2 + \frac{1}{4}\left(f_{j-2} - 4f_{j-1} + 3f_j\right)^2, \\ \beta_1 = \frac{13}{12}\left(f_{j-1} - 2f_j + f_{j+1}\right)^2 + \frac{1}{4}\left(f_{j-1} - f_{j+1}\right)^2, \\ \beta_2 = \frac{13}{12}\left(f_j - 2f_{j+1} + f_{j+2}\right)^2 + \frac{1}{4}\left(3f_j - 4f_{j+1} + f_{j+2}\right)^2. \end{cases} \tag{16}$$

There are many methods proposed [6, 7, 8] to improve the performance of WENO-JS scheme. For example, Borgers et al. [7] introduced the global smoothness indicator τ_5 to calculate the weights and the proposed WENO-Z scheme has less dissipation and higher resolution than WENO-JS scheme. The un-normalized weights α_k^z of WENO-Z scheme are calculated as

$$\alpha_k^z = c_k\left(1 + \frac{\tau_5}{\beta_k + \varepsilon}\right), \quad \tau_5 = \left|\beta_0 - \beta_2\right|, \quad k = 0, 1, 2. \tag{17}$$

The global smoothness indicator τ_5 has the following properties [9]:

(1) For a stencil $S^5 = (x_{j-2}, x_{j-1}, \ldots, x_{j+2})$, if S^5 does not contain discontinuities, then $\tau_5 \ll \beta_k$ for $k = 0, 1, 2$;

(2) If the solution is continuous at some of the stencil S_k^3, but discontinuous in the whole stencil S^5, then for the smooth stencils, $\beta_k \ll \tau_5$;

(3) $\tau_5 \leqslant \max\left(\beta_0, \beta_1, \beta_2\right)$.

Following the above properties, Shen and Zha [9] proposed a detecting method for a non-smooth stencil, that is:

If $\tau_5 > \min\left(\beta_0, \beta_1, \beta_2\right)$, then S^5 is a non-smooth stencil.

2.3 The analysis of characteristic-wise WENO reconstruction based on FVS

If a characteristic-wise reconstruction method is used to reconstruct $\mathbf{F}_{j+1/2}^+$ and $\mathbf{F}_{j+1/2}^-$, all the characteristic variables of $\mathcal{F}_j^+$ and $\mathcal{F}_j^-$ on the used global stencil are first calculated. For brevity, only the reconstruction of $\mathbf{F}_{j+1/2}^+$ (the five-point global stencil $S^5 = (j-2, j-1, ..., j+2)$ is used for a fifth-order WENO reconstruction) is discussed. Noted that, for $F_{j+1/2}^-$, point $j+3$ is needed. The local characteristic variables $\mathcal{F}_i^+$ $(i = j-2, ..., j+2)$ on the stencil S^5 are

$$\mathcal{F}_i^+ = \left[\ \mathfrak{f}_1, \mathfrak{f}_2, \mathfrak{f}_3\ \right]_i^T = \hat{L}_{j+1/2} F_i^+ = \begin{bmatrix} \dfrac{\lambda_* p}{2\hat{c}^2} - \dfrac{\lambda_{**}\rho c}{2\gamma\hat{c}} \\ -\dfrac{\lambda_* p}{\hat{c}^2} + f_1^+ \\ \dfrac{\lambda_* p}{2\hat{c}^2} + \dfrac{\lambda_{**}\rho c}{2\gamma\hat{c}} \end{bmatrix}_i, \tag{18}$$

where f_1^+ is the split flux of f_1 in Eq. (7), and

$$\lambda_* = \frac{\lambda_3^+ + \lambda_1^+}{2}, \quad \lambda_{**} = \frac{\lambda_3^+ - \lambda_1^+}{2}. \tag{19}$$

The values $(\hat{\cdot})$ in the matrix $\hat{L}_{j+1/2}$ are calculated by a certain averaged method of nodes j and $j+1$ (in this paper, the simple mean is used). If a fifth-order WENO scheme is used to reconstruct the characteristic variables, the reconstructed values can be calculated as

$$\mathcal{F}^{+}_{j+1/2} = \begin{bmatrix} \sum_{k=0}^{2}[\omega_k(\mathfrak{f}_1)Q_k(\mathfrak{f}_1)] \\ \sum_{k=0}^{2}[\omega_k(\mathfrak{f}_2)Q_k(\mathfrak{f}_2)] \\ \sum_{k=0}^{2}[\omega_k(\mathfrak{f}_3)Q_k(\mathfrak{f}_3)] \end{bmatrix} = \begin{bmatrix} \frac{1}{2}\sum_{k=0}^{2}[\omega_k(\mathfrak{f}_1)Q_k(\frac{\lambda_* p}{\hat{c}^2})] - \frac{1}{2}\sum_{k=0}^{2}[\omega_k(\mathfrak{f}_1)Q_k(\frac{\lambda_{**}\rho c}{\gamma\hat{c}})] \\ -\sum_{k=0}^{2}[\omega_k(\mathfrak{f}_2)Q_k(\frac{\lambda_* p}{\hat{c}^2})] + \sum_{k=0}^{2}[\omega_k(\mathfrak{f}_2)Q_k(f_1^{+})] \\ \frac{1}{2}\sum_{k=0}^{2}[\omega_k(\mathfrak{f}_3)Q_k(\frac{\lambda_* p}{\hat{c}^2})] + \frac{1}{2}\sum_{k=0}^{2}[\omega_k(\mathfrak{f}_3)Q_k(\frac{\lambda_{**}\rho c}{\gamma\hat{c}})] \end{bmatrix}, \tag{20}$$

where $\omega_k(\mathfrak{f}_l)$ and $Q_k(\mathfrak{f}_l)$ $(l = 1, 2, 3)$ are the weights and linear candidate reconstructions calculated by using the characteristic variable $\mathfrak{f}_l$ on the sub-stencil $S_k = (j-2+k, ..., j+k)$, respectively.

The final numerical flux are obtained by

$$F^{+}_{j+1/2} = \widehat{R}_{j+1/2}\mathcal{F}^{+}_{j+1/2}. \tag{21}$$

2.3.1 Different performances between SW and LF-type splitting methods

Without loss of generality, suppose that a contact discontinuity is located between the nodes $j+1$ and $j+2$ (see Fig. 1), and the velocity and pressure can be set as

$$u = u_o, \quad p = p_o. \tag{22}$$

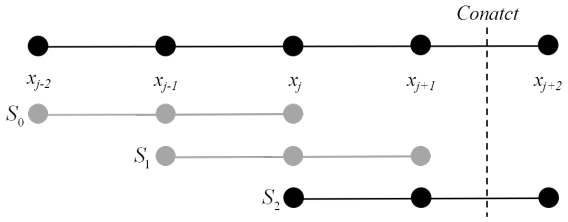

Figure 1: Stencil with a contact at the third sub-stencil

Combining with $c_i^2 = \dfrac{\gamma p_i}{\rho_i}$, the expressions for the characteristic variables in Eq. (18) calculated by using the different flux vector splitting methods at different Mach numbers (M) are listed in Table 1. From the table, the following information can be obtained:

(1) Case $1: |M| > 1$

For both the SW-FVS and GLF-FVS methods, the characteristic variables $\mathfrak{f}_1$ and $\mathfrak{f}_3$ are constants on the global stencil S^5 shown in Fig. 1, hence the weights calculated by them are the ideal weights. While, the weights calculated by $\mathfrak{f}_2$ give different weight distributions. For convenience, we give these approximate weights in Table 2. Therefore, Eq. (20) can be written as

$$F^+_{j+1/2} = \widehat{R}_{j+1/2}\mathcal{F}^+_{j+1/2} = \sum_{k=0}^{2} \omega_k^* Q_k(F^+) + \xi S_{j+1/2}, \tag{23}$$

where

$$\omega_k^* = \frac{\omega_k(\mathfrak{f}_1) + \omega_k(\mathfrak{f}_3)}{2}, \quad \xi = (1, u, u^2/2)^T, \quad S_{j+1/2} = \sum_{k=0}^{2}[(\omega_k^* - \omega_k(\mathfrak{f}_2))Q_k(\mathfrak{f}_2)], \tag{24}$$

and

$$|\omega_k^* - \omega_k(\mathfrak{f}_2)| = O(1),\ (k = 0, 1, 2). \tag{25}$$

The second term $\xi S_{j+1/2}$ of the right-hand side of Eq. (23) can be regarded as a modified term for the WENO reconstructions of the split flux F^+.

Eq. (25) shows that, the modified term $\xi S_{j+1/2}$ cannot be neglected, and this is the actual difference between the characteristic-wise reconstruction and the component-wise reconstruction.

(2) Case 2 : $|M| < 1$

For the SW-FVS method, all the characteristic variables $\mathfrak{f}_l$ ($l = 1, 2, 3$) are discontinuous across the contact discontinuity, and the approximate weights (also see Table 2) have the same magnitude of order, that is

$$|\omega_k(\mathfrak{f}_m) - \omega_k(\mathfrak{f}_n)| = O(\epsilon),\ (k, m, n = 0, 1, 2). \tag{26}$$

Hence, the effects of the modified term $\xi Sj + 1/2$ plays a negligible role on the reconstruction, and the characteristic-wise reconstruction becomes close to the component-wise flux reconstruction

$$F^+_{j+1/2} = \sum_{k=0}^{2} \omega_k^* Q_k(F^+) + O(\epsilon). \tag{27}$$

On the other hand, the GLF-FVS methods still can keep the relationship of Eq. (25).

Table 1: The variables near contact discontinuities.

Splitting method	M	λ_*	λ_{**}	$\mathfrak{f}_1$	$\mathfrak{f}_2$	$\mathfrak{f}_3$
SW	$M > 1$	u	c	$\frac{up}{2\hat{c}^2} - \frac{p}{2\hat{c}}$	$\frac{-up}{\hat{c}^2} + f_1^+$	$\frac{up}{2\hat{c}^2} + \frac{p}{2\hat{c}}$
	$0 < \lvert M\rvert < 1$	$\frac{u+c}{2}$	$\frac{u+c}{2}$	$\frac{(u+c)p}{4\hat{c}^2} - \frac{\rho uc}{4\gamma\hat{c}} - \frac{p}{4\hat{c}}$	$\frac{(u+c)p}{2\hat{c}^2} + f_1^+$	$\frac{(u+c)p}{4\hat{c}^2} + \frac{\rho uc}{4\gamma\hat{c}} + \frac{p}{4\hat{c}}$
	$M < -1$	0	0	0	f_1^+	0
GLF	$M \in \mathbb{R}$	$\frac{u+\alpha}{2}$	$\frac{c}{2}$	$\frac{(u+\alpha)p}{4\hat{c}^2} - \frac{p}{4\hat{c}}$	$\frac{-(u+\alpha)p}{2\hat{c}^2} + f_1^+$	$\frac{(u+\alpha)p}{4\hat{c}^2} + \frac{p}{4\hat{c}}$

Table 2: The approximate weights of the substencils in Fig. 1.

Splitting method	M	k	$\omega_k(\mathfrak{f}_1)$	$\omega_k(\mathfrak{f}_2)$	$\omega_k(\mathfrak{f}_3)$
SW	$\|M\|>1$	0	$1/10$	$1/7$	$1/10$
		1	$6/10$	$6/7$	$6/10$
		2	$3/10$	0	$3/10$
	$\|M\|<1$	0	$1/7$	$1/7$	$1/7$
		1	$6/7$	$6/7$	$6/7$
		2	0	0	10
GLF	$M\in\mathbb{R}$	0	$1/10$	$1/7$	$1/10$
		1	$6/10$	$6/7$	$6/10$
		2	$3/10$	0	$3/10$

2.3.2 A new characteristic-wise WENO scheme based on a hybrid FVS method

The analysis of Sec. 2.3.1 shows that, for the case of subsonic contact discontinuities, even the characteristic-wise WENO scheme based on the SW-FVS method may lose the local property of characteristic-wise (it performs similarly as the component-wise flux reconstruction), and hence the method may results in spurious numerical oscillations near the subsonic contact discontinuities.

To keep the local property of characteristic-wise for the subsonic contact discontinuities and obtain the low dissipative solution in other regions, we propose a new characteristic-wise WENO scheme based on a hybrid FVS method.

First, we detect the trouble stencil (of discontinuous and subsonic) by combining the τ_5 detecting method ($\tau_5 > min(\beta_0, \beta_1, \beta_2)$) [9] and the Mach number, then for the characteristic-wise WENO reconstruction on this stencil (for example, S^5=$(j-2, j-1, ..., j+2)$), the split fluxes ($F_{j-2}^{GLF,\pm}, ..., F_{j+2}^{GLF,\pm}$) of GLF-FVS are used to obtain the final numerical flux $F_{j\pm1/2}$. For the other normal stencils, the split fluxes of SW-FVS are used

For convenience, the new method (take $F_{j+1/2}^{+}$ as an example, and the stencil for a fifth order WENO scheme is $S^5 = (j-2, .., ..j+2)$) is briefly given in Algorithm 1.

Algorithm 1 Algorithm

DO j=1 to N

1. Detecting and flux vector splitting

if $\tau_5 > min(\beta_0, \beta_1, \beta_2)$ (calculated by desity) and $|M_{j+1/2}| < 1$

for $j-2 \le i \le j+2$

$\mathcal{F}_i^+ = \hat{L}_{j+1/2} F_i^{GLF,+}$,

end for

else

for $j-2 \le i \le j+2$

$\mathcal{F}_i^+ = \hat{L}_{j+1/2} F_i^{SW,+}$,

end for

end if

2. WENO reconstruction and the final numerical flux

$$\mathcal{F}_{j+1/2}^+ = \begin{bmatrix} \sum_{k=0}^{2} [\omega_k(\mathfrak{f}_1) Q_k(\mathfrak{f}_1)] \\ \sum_{k=0}^{2} [\omega_k(\mathfrak{f}_2) Q_k(\mathfrak{f}_2)] \\ \sum_{k=0}^{2} [\omega_k(\mathfrak{f}_3) Q_k(\mathfrak{f}_3)] \end{bmatrix},$$

$F_{j+1/2}^+ = \widehat{R}_{j+1/2} \mathcal{F}_{j+1/2}^+$.

END DO

3 NUMERICAL EXAMPLES

In this paper, the 3th order Runge–Kutta-type method [10] is used for the time marching. In the figures, the results of the component-wise WENO scheme directly weighting the split fluxes of the GLF-FVS method are denoted as CP; those of the characteristic-wise WENO scheme based on three different flux splitting methods are denoted as GLF, SW, and Present, respectively.

3.1 The Sod-type problems

The initial conditions of a pair of Sod-type problems [11, 12] are given by:

$$\text{Case 1} : (\rho, u, p) = \begin{cases} (1, 0, 1), & 0 \le x \le 0.5, \\ (0.125, 0, 0.1), & 0 < x \le 1; \end{cases}$$

$$\text{Case 2} : (\rho, u, p) = \begin{cases} (1, 1.25, 1), & 0 \le x \le 0.3, \\ (0.125, 0, 0.1), & 0.3 < x \le 1. \end{cases}$$

The final solution times are $t = 0.14$ and 0.2 for the two sets of initial values, respectively. The zero gradient boundary conditions are used. The solutions with the grid of N = 200 are given in Figs. 2 and 3.

(1) In the both cases, the component-wise WENO scheme (the directly weighting for the split flux of the GLF method, denote as CP in the figures) generates oscillations. (2) The characteristic-wise WENO scheme based on the SW-FVS method (denoted as SW in the figures) generates overshoots in the subsonic case ($|M| < 1$, Fig.3) and does not in the supersonic case ($|M| > 1$, Fig.4), that is in agreement with the above analysis in Sec. 2.3.1. (3) Both the characteristic-wise WENO scheme of GLF-FVS and the prerent hybrid FVS (denoted as GLF and present) do not generate spurious solutions, the present method is less dissipative than GLF.

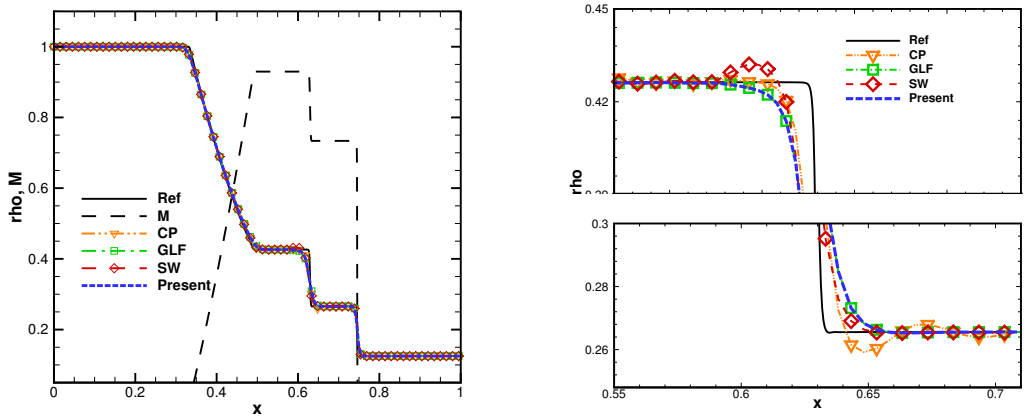

Figure 2: Solutions of the Sod problem (Case 1).

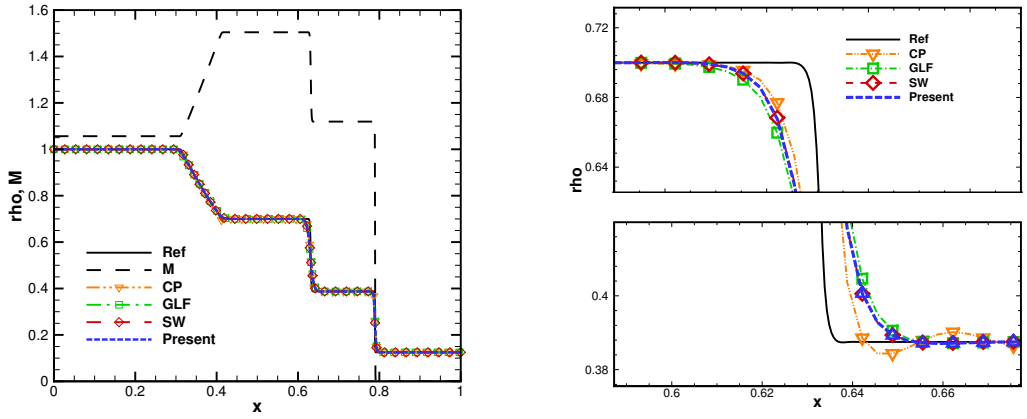

Figure 3: Solutions of the Sod problem (Case 2).

3.2 The Lax-type problems

The initial conditions of a pair of Lax-type problems [13, 12] are given by:

$$\text{Case } 1: (\rho, u, p) = \begin{cases} (0.445, 0.698, 3.528), & -1 \le x \le 0, \\ (0.5, 0, 0.571), & 0 < x \le 1; \end{cases}$$

$$\text{Case } 2: (\rho, u, p) = \begin{cases} (0.445, 6.98, 3.528), & -1 \le x \le -0.6, \\ (0.5, 0, 0.571), & -0.6 < x \le 1. \end{cases}$$

The final solution times are $t = 0.26$ and 0.245 for the two sets of initial values, respectively. The zero gradient boundary conditions are used. The solutions with the grid of N = 300 are given in Figs. 4 and 5, which include the subsonic and supersonic contact discontinuity respectively. As the previous conclusions, the present method can prevent oscillations and shapely capture contact discontinuities.

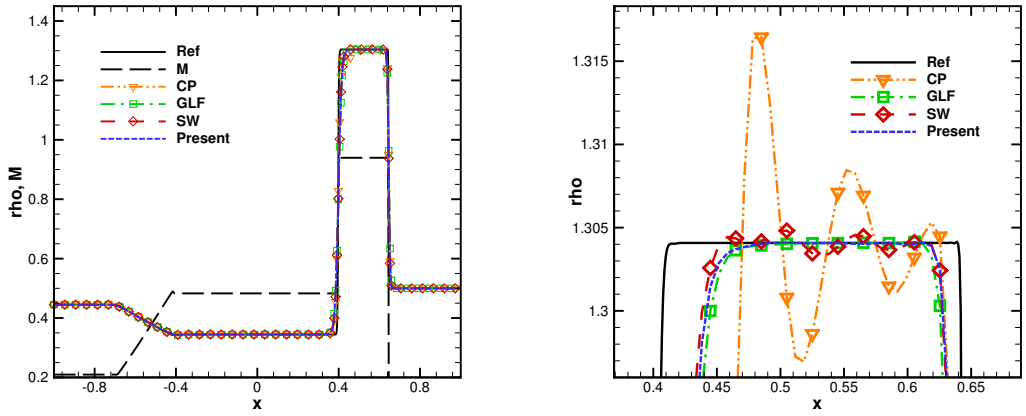

Figure 4: Solutions of the Lax problem (Case 1).

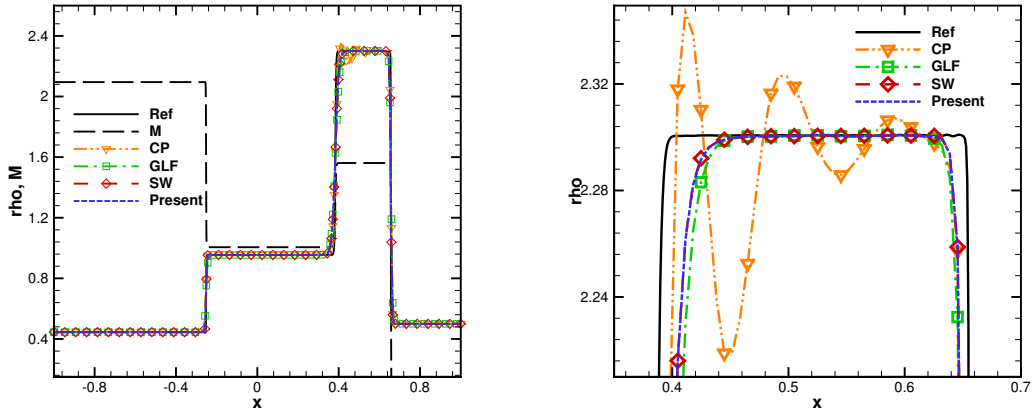

Figure 5: Solutions of the Lax problem (Case 2).

3.3 The Shu-Osher problem

The initial conditions of the Shu-Osher problem [2] are

$$(\rho, u, p) = \begin{cases} (3.857143, 2.629369, 31/3), & -5 \le x \le -4, \\ (1 + 0.2\sin(5x), 0, 1), & -4 < x \le 5. \end{cases}$$

The final solution time is $t = 1.8$ and the zero gradient boundary conditions are used. The solutions are given in Figs. 6 and 7. It can be seen that, CP method overshoots as grid refining. The present, as the SW method, has higher resolution and less dissipation properties in smooth regions.

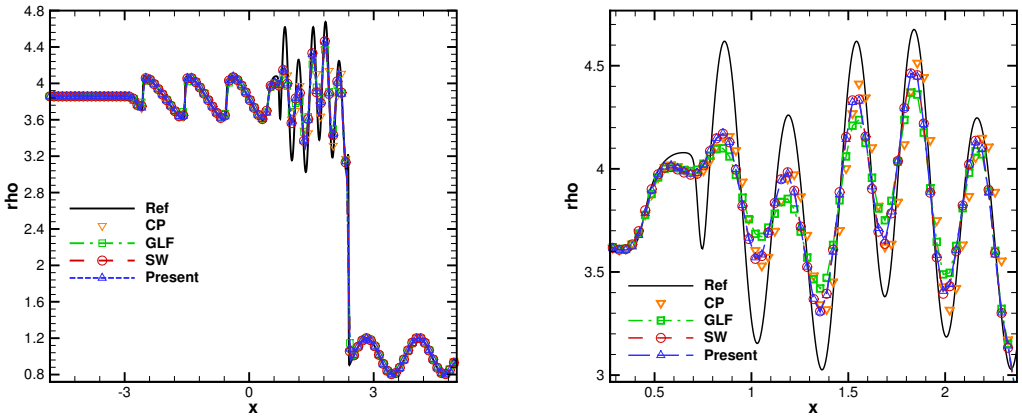

Figure 6: Solutions of the Shu-Osher problem with $N = 300$.

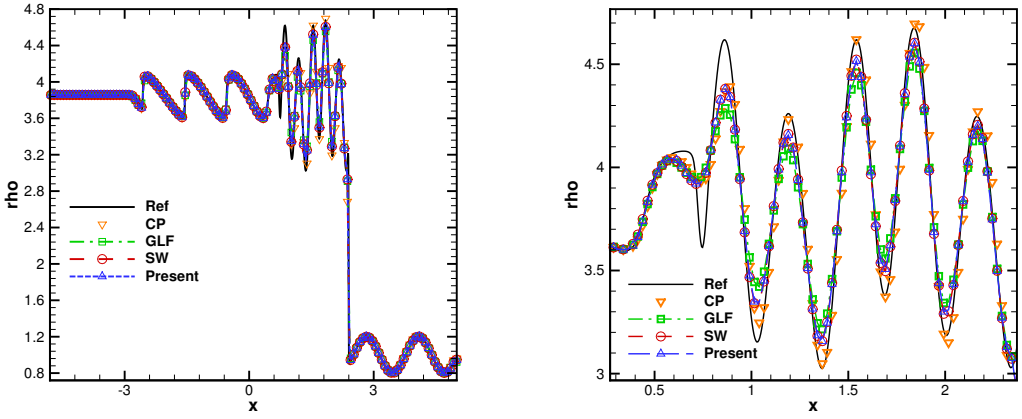

Figure 7: Solutions of the Shu-Osher problem with $N = 400$.

4 CONCLUSIONS

In this paper, the reason of the oscillation near the subsonic contact discontinuities caused by the characteristic-wise WENO reconstruction based on the SW-FVS method is analyzed. Then a characteristic-wise WENO reconstruction based on the hybrid FVS method is proposed. Numerical results are presented to show the new method can effectively suppress the oscillation near the subsonic contact discontinuities and also keep the low-dissipation and high-resolution as that of SW-FVS in other regions .

Acknowledgement

This research was supported by the National Natural Science Foundation of China under Grants Nos. 12172364, 11872067 and 91852203.

REFERENCES

[1] S. L. Steger, R. F. Warming, Flux vector splitting of the inviscid gasdynamic equations with application to finite-difference methods, J. Comput. Phys. 40 (2) (1981) 263–293.

[2] C.-W. Shu, S. Osher, Efficient implementation of essentially non-oscillatory shock-capturing schemes, II, J. Comput. Phys. 83 (1) (1989) 32–78.

[3] J. Qin, Y. Shen, Y. Cheng, B. Zhou, A modified characteristic-wise WENO reconstruction for capturing the contact discontinuity in multi-component flows, Submitted to publisher. Available at SSRN: https://ssrn.com/abstract=4621573.

[4] G.-S. Jiang, C.-W. Shu, Efficient implementation of weighted ENO schemes, J. Comput. Phys. 126 (1) (1996) 202–228.

[5] E. Johnsen, On the treatment of contact discontinuities using WENO schemes, J. Comput. Phys. 230 (24) (2011) 8665–8668.

[6] A. K. Henrick, T. A. Aslam, J. M. Powers, Mapped weighted essentially non-oscillatory schemes: achieving optimal order near critical points, J. Comput. Phys. 207 (2) (2005) 542–567.

[7] R. Borges, M. Carmona, B. Costa, W. S. Don, An improved weighted essentially non-oscillatory scheme for hyperbolic conservation laws, J. Comput. Phys. 227 (6) (2008) 3191–3211.

[8] Y. Shen, G. Zha, Improvement of weighted essentially non-oscillatory schemes near discontinuities, Comput. Fluids 96 (2014) 1–9.

[9] Y. Shen, G. Zha, Generalized finite compact difference scheme for shock/complex flow-field interaction, J. Comput. Phys. 230 (12) (2011) 4419–4436.

[10] C.-W. Shu, S. Osher, Efficient implementation of essentially non-oscillatory shock-capturing schemes, J. Comput. Phys. 77 (2) (1988) 439–471.

[11] P. Wesseling, Principles of computational fluid dynamics, Vol. 29, Springer Science & Business Media, 2009.

[12] E. F. Toro, Riemann solvers and numerical methods for fluid dynamics: A practical introduction, 2009.

[13] P. D. Lax, Weak solutions of nonlinear hyperbolic equations and their numerical computation, Commun. Pure Appl. Math. 7 (1) (1954) 159–193.